Analysis of the intermediate-band absorption properties of type-II GaSb/GaAs quantum-dot photovoltaics

I. Ramiro, J. Villa, C. Tablero, E. Antolín, A. Luque, A. Martí, J. Hwang, J. Phillips, A. J. Martin, and J. Millunchick

Analysis of the Intermediate-Band Absorption Properties of Type II GaSb/GaAs Quantum-Dot Photovoltaics

I. Ramiro[,†], J. Villa, C. Tablero, E. Antolín, A. Luque, and A. Martí

Instituto de Energía Solar, Universidad Politécnica de Madrid, 28040 Madrid, Spain

J. Hwang[‡] and J. Phillips

Dept. of Electrical Engineering and Comp. Sci., University of Michigan, Ann Arbor MI 48109, USA

A.J. Martin and J. Millunchick

Dept. of Materials Science and Engineering, University of Michigan, Ann Arbor MI 48109, USA

Quantum-dot (QD) intermediate-band (IB) materials are regarded as promising candidates for high-efficiency photovoltaics. The sequential two-step two-photon absorption processes that take place in these materials have been proposed to develop high-efficiency solar cells and infrared (IR) photodetectors. In this work, we experimentally and theoretically study the interrelation of the absorptivity with transitions of carriers to and from the IB in type II GaSb/GaAs QD devices. Our devices exhibit three optical bandgaps with: E_L=0.49 eV, E_H=1.02 eV and E_G=1.52 eV, with the IB located 0.49 eV above the valence band. These values are well supported by semi-empirical calculations of the QDs electronic structure. Through intensity-dependent two-photon photocurrent experiments, we are able to vary the filling state of the IB, thus modifying the absorptivity of the transitions to and from this band. By filling the IB with holes via E=1.32 eV or E=1.93 eV monochromatic illumination, we demonstrate an increase in the E_L–related absorptivity of more than two orders of magnitude and a decrease in the E_H–related absorptivity of one order of magnitude. The anti-symmetrical evolution of those absorptivities is quantitatively explained by a photo-induced shift of the quasi-Fermi level of the IB. Furthermore, we report the observation of a two-photon photovoltage; i. e., the contribution of sub-bandgap two-photon absorption to increase the open-circuit voltage of solar cells. We find that the generation of the two-photon photovoltage is related, in general, to the production of a two-photon photocurrent. However, while photons with energy close to E_L participate in the production of the two-photon photocurrent, they are not effective in the production of a two-photon photovoltage. We also report the responsivity of GaSb/GaAs QD devices performing as optically triggered photodetectors. These devices exhibit an amplification factor of almost 400 in the IR spectral region. This high value is achieved by minimizing –via doping– the absorptivity in the IR range of the QDs under equilibrium conditions.

I. INTRODUCTION

[,] i.ramiro@ies.upm.es

[†] Now with ICFO – The Institute of the Photonic Sciences, Barcelona, Spain.

[‡] Now with School of Electronics and Information Engineering, Korea Aerospace University, 10545 Goyang-si, Republic of Korea.

In the last decades, great effort has been devoted to the design of new device architectures and engineering new materials for achieving low-cost high-efficiency photovoltaics [1]. One attractive approach is intermediate band (IB) materials [2]. An IB material is a semiconductor with an electronic structure where a third electronic band, the IB, exists between the valence band (VB) and the conduction band (CB). The presence of the IB creates two new sub-bandgaps, E_H and E_L, with higher and lower energies, respectively, in addition to the fundamental bandgap, E_G (Figure 1a). Therefore, the IB allows electron interaction with sub-bandgap energy (E) photons ($E < E_G$) by means of carrier generation and recombination processes. Of particular interest is the generation of electron-hole pairs —with one electron in the CB and one hole in the VB— through the sequential absorption of two photons of different energy, with at least one of the photons having energy lower than the bandgap energy E_G. These two-step two-photon processes are sketched in Figure 1a. Process (I) consists of electron-hole pair generation via the absorption of two sub-bandgap photons, one of them with $E > E_H$ (pumping one electron from the VB to the IB) and the other, with $E > E_L$, pumping one electron (not necessarily the same one) from the IB to the CB. In this case, the IB acts as a "stepping-stone" to promote a net electron to the CB. The exploitation of this two-photon mechanism for harvesting sub-bandgap photons and increasing the conversion efficiency of solar cells was first proposed in Ref. [3] and then revised and completed in Ref. [2], where the conversion efficiency of an ideal system was calculated. This led to the research on the field of the so-called intermediate band solar cells (IBSCs) [4–6]. In process (II), one photon has energy above the bandgap energy ($E > E_G$) while the second one exhibits sub-bandgap energy ($E > E_L$). Through the absorption of the above-bandgap photon, an electron-hole pair is created. However, for the case of Figure 1a, the electron in the CB may relax to the IB. In this situation, the absorption of the sub-bandgap second photon pumps the electron back to the CB and restores the electron-hole pair. The exploitation of this two-photon process for infrared (IR) light detection was first proposed and demonstrated in Ref. [7], opening up a new line of research on the so-called optically-triggered infrared photodetectors (OTIPs).
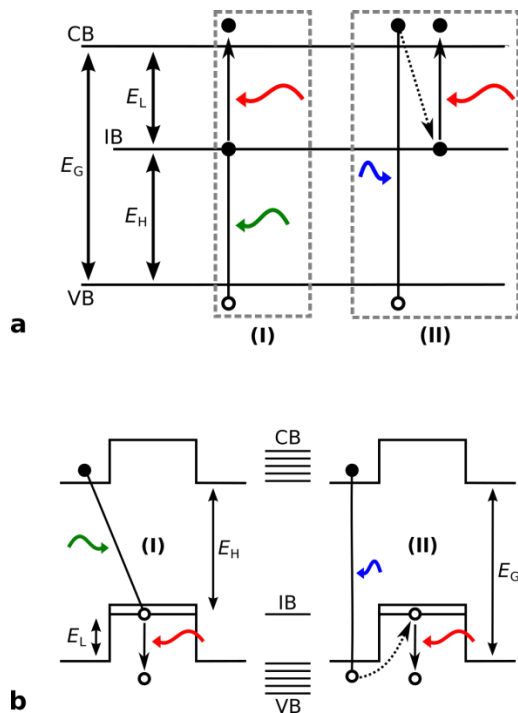

Figure 1. Two-step two-photon processes. (a) In a generic IB material. Process (I) consists of the generation of an electron-hole pair due to the absorption of two sub-bandgap photons, one of them with $E > E_H$ and the other with $E > E_L$. Process (II) consists of the

generation of an electron-hole pair due to the absorption of one above-bandgap ($E > E_G$) photon and one sub-bandgap photon with $E > E_L$. **(b)** In GaSb/GaAs QDs. The type-II band lineup of GaSb/GaAs QDs is illustrated. In process (I) one photon pumps an electron from the IB to the CB and, subsequently, a hole confined in the IB is pumped by another photon to the VB. In process (II) one electron-hole pair is created by one photon. The hole relaxes into the less energetic IB and is subsequently pumped back into the VB by a second photon.

Different technological approaches have been investigated in order to manufacture IB devices [5]. The most common approach is semiconductor quantum dots (QDs). Under this approach, the IB is formed by the confined electronic states introduced by the QDs amidst the host semiconductor bandgap. So far, the vast majority of QD-IB prototypes have been implemented using type I (straddling band lineup, see Figure 2) QDs; in particular, QDs systems in which the IB is taken as the most confined electronic states in the conduction band of the QD material. For this reason, we say that these are *electron-based* systems. The first demonstration of process (I) was reported in the InAs/GaAs QD system [8]. Since then, it has also been reported in other QD systems, such as GaAs/AlGaAs [9] and InAs/AlGaAs [10,11]. Recently, the demonstration of process (I) in a single InAs/GaAs QD has been reported [12]. Process (II) was first reported in InAs/AlGaAs QDs [7].
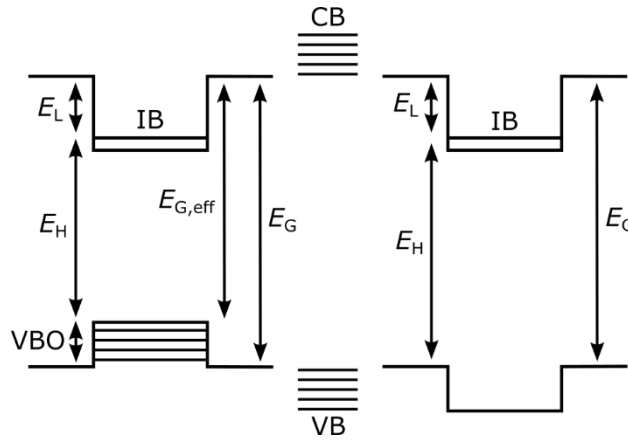

Figure 2. Simplified band diagram of electron-based type-I (left) and type-II (right) QD-IB materials. $E_{G,eff}$ is the effective bandgap in terms of maximum attainable V_{OC} in type-I QD-IBSCs. The electron-based IB is represented with a single level in the conduction band potential well of the QDs. The non-zero density of states of holes in the QDs is indicated with horizontal lines.

Regarding the implementation of QD-IBSCs – that have been much more extensively studied than OTIPs – several practical problems have been encountered. One major concern is the open-circuit voltage (V_{OC}). In ideal IBSCs, the effect of the IB should be an increase in the photo-generated current with a minimal reduction in V_{OC} [2]. However, most of the fabricated devices exhibited low V_{OC} [5]. The voltage degradation in QD-IBSC prototypes is attributed to different causes: (1) non-radiative recombination caused by the strain-induced structural defects in the QD stack. To reduce structural defects, different techniques, such as increasing the thickness of the barriers between QD layers [13] and including strain-compensating layer [14–17], have been implemented, which led to QD-IBSC prototypes exhibiting almost non-degraded V_{OC} [18]. (2) Thermal generation-recombination mechanisms connecting the IB and the CB. To reduce the IB-CB thermal connection, QD systems with larger E_L are being investigated [19–24]. (3) Tunneling transport between the IB and the CB. This problem has been addressed by reducing the electric field in the QD region, either by increasing the thickness of spacers [25] or by including field damping layers [26]. (4) The fast capture of photo-excited electrons into the potential well of the QDs. Electronic doping of the dots have been proposed a way of

creating a built-in-dot charge, thus hampering the electron capture [27]. Notwithstanding these efforts, it has been argued that the type-I band diagram may result in a fundamental limitation to the maximum attainable V_{OC} [28,29]. For example, in the case of electron-based type-I systems, the valence band offset (VBO) (see Figure 2) is believed to produce an effective bandgap narrowing in terms of maximum attainable V_{OC}. Under this line of thought, the V_{OC} limitation would be similar to that occurring when a lower bandgap material is used as a barrier material between QD layers [30]. It has been suggested that type-II (staggered band lineup, Figure 2) QDs may be advantageous for the implementation of IBSCs, since they would not cause effective bandgap narrowing [29]. In the past years, various experimental works on type-II QD-IBSCs have been reported [31–36]. In Refs. [35,36] and [34], process (I) and (II), respectively, were demonstrated. All those works employed GaSb/GaAs QDs as the IB material.

GaSb/GaAs QDs exhibit a type-II band lineup with confinement of holes only [37–39], as depicted in Figure 1b. Hence, we say that this IB material is *hole-based*. For the sake of simplicity, only the deepest confined hole state —the ground state— has been represented in Figure 1b. Note that in this material the IB is closer to the VB than to the CB, and the sub-bandgaps E_H and E_L are denoted accordingly. Figure 1b also illustrates how two-photon processes (I) and (II) (described for the general case in Figure 1a) take place in GaSb/GaAs QDs.

The basic two-photon-absorption phenomena have been, therefore, demonstrated in both type-I and type-II, and both electron-based and hole-based QD systems. Nonetheless, some fundamental questions regarding multi-photon absorption processes need to be answered before practical IB devices may be developed: How does absorption of light in one of the three bandgaps (E_G, E_H or E_L) impact the absorption strength of the other bandgaps? What is the role of the density of states of the IB? In this work, we study the multi-photon absorption properties of a hole-based IB consisting of type-II GaSb/GaAs QDs by means of two-photon photocurrent and two-photon photovoltage experiments. We show that the rate of two-photon processes is dependent on the intensities of the two light beams. Light-intensity-dependent studies allow us to reveal that the absorption strength related to sub-bandgap transitions is dependent on the electron occupancy of the IB. By high photo-filling (with holes) in the IB, we are able to demonstrate photon absorption involving shallow (close to the VB) confined states in GaSb/GaAs QDs. In this respect, we report the generation of (two-photon) photocurrent response for photon energies as low as 0.2 eV, while the energy difference between the VB and the ground state is 0.49 eV. In addition, we demonstrate the production of a two-photon photovoltage; i. e., the increase in the V_{OC} of a solar cell due to sub-bandgap two-photon absorption, demonstrating that this below bandgap absorption also contributes to the split of quasi-Fermi levels. Our experimental results, sustained by computational simulations, allow us to draw a theoretical framework of the multi-photon absorption properties of the studied IB. The proposed theoretical modeled successfully explains the experimental results.

II. SAMPLES AND METHODS

IB devices with a p+/n-/n structure including 10 layers of GaSb/GaAs QDs in the n- region were fabricated to study the IBSC and the OTIP framework. Their semiconductor layer structure is sketched in Figure 3a. Samples were grown by molecular beam epitaxy (MBE) on heavily doped n-GaAs (100) substrates. GaSb QDs were grown via the Stranski-Kranstanov growth mode with 2.3ML nominal thickness of a GaSb layer on an Sb-terminated (2x8) surface reconstruction. All QD layers were immediately capped by 30 nm of GaAs. Samples consist of a GaAs p-n junction with the QD-stack in the n-side near the junction. AlGaAs window and back-surface-field layers were grown on top of and below the p-GaAs and the n-GaAs emitters, respectively, in order to minimize carrier recombination at the interfaces with the metallic contacts. Device structures were fabricated using standard photolithography, metallization, and etching techniques. The full layer structure of the diode is described in Supplemental Material Figure S1.

The MBE grown GaAs p-n junctions were fabricated into square solar cells of area 6.84 mm^2. All devices were mesa isolated, with ohmic metal contacts provided by Pd/Zn/Pd/Au and Ni/Ge/Au/Ti/Au for p-type and n-type GaAs, respectively, followed by rapid thermal annealing at 400°C. An anti-reflection coating of ZnS and MgF$_2$ was deposited on the top surface.
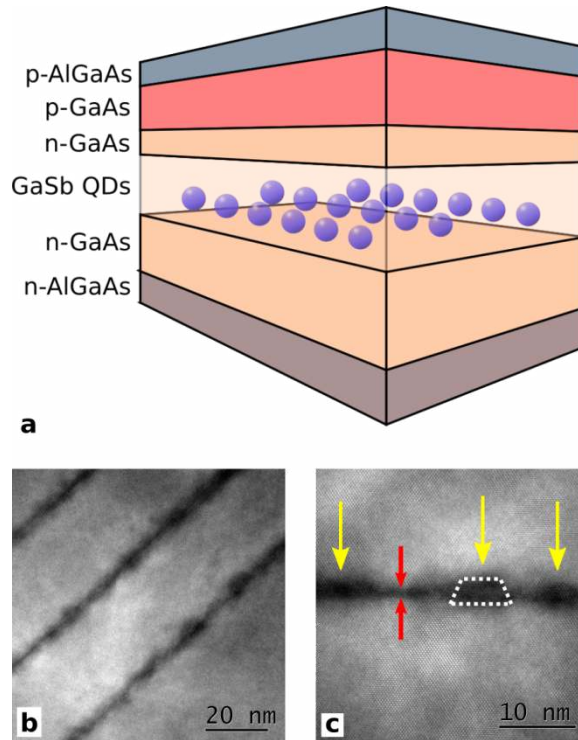

Figure 3. Fabricated GaSb/GaAs IB samples. (a) Semiconductor layer structure of the fabricated samples. The QD stack consists of 10 layers of GaSb QDs. (b,c) HRTEM micrographs showing: (b) three consecutive QD layers and (c) a magnification of one QD layer. Zones rich in Sb appear darker in the images than zones rich in As. The big yellow arrows in (c) point at the GaSb QDs. The small red arrows delimit the width of the GaSb wetting layer. Horizontal bars indicate the scale of the images. A dotted white line, encircling a trapezoid, depicts the cross section of one QD as modeled in Section II.D.

The HRTEM images shown in Figure 3 were performed in a S-Twin Tecnai G2-F30 Field Emission Gun microscope with a super-twin lens and 0.2 nm point-to-point resolution and 0.1 line resolution, operated at 300kV.

The two-photon photocurrent (TPPC) and photovoltage measurements were performed using the same set-up with slight modifications. A sketch of the employed experimental set-up can be found in Ref. [7]. Samples were mounted on a closed-cycle He-cryostat. Two light sources could simultaneously illuminate the samples. IR illumination "ph1" (a SiC lamp) was chopped and directed into a three-grating 1/4 m monochromator. A set of IR long-pass optical filters was placed at the exit of the monochromator to minimize the impact of residual broadband and second-order light on the measurements. "ph2" is a monochromatic source which could be switched on and off. Final signal detection was made using a dual-phase lock-in amplifier. For the two-photon photocurrent (TPPC) measurements, ph2 was either 1.93-eV LED or a 1.32-eV laser diode; samples were connected to a low-noise transimpedance amplifier, which also served as voltage source to short-circuit the samples; and the chopping frequency was 23 Hz. The method for converting the measured photocurrent into QE or SR is detailed in Ref. [36]. For the photovoltage measurements, only the 1.32 eV source was employed; samples were connected to a voltage amplifier; and the chopping frequency was 6 Hz.

For the electroluminescence measurements, samples were mounted on a closed-cycle He-cryostat and excited with modulated current provided by a current source. The emitted light was directed onto a two-grating 1/8 m monochromator. Light detection was done with calibrated Si and Ge detectors. Conventional lock-in techniques were used for measuring the electrical response of the detectors.

III. RESULTS AND DISCUSSION

A. Structural characterization

Figure 3b and Figure 3c show cross-sectional high-resolution transmission electron microscopy (HRTEM) images of the QD stack of one of the samples. Figure 3b shows the first three layers (from bottom to top in the structure) of GaSb QDs. A high density of closely spaced QDs is deduced from the image with an inhomogeneous size distribution. From measurements in previous growths, we estimate an areal density on the order of 10^{10} cm^{-2}. Most QDs have a lateral size smaller or equal to 10 nm, while the QD height is in the range of 3–4 nm. These size values will be used for the calculations performed in Section III.D. A single QD layer is shown in Figure 3c, where the yellow arrows point at the GaSb QDs, while the red arrows indicate the width of the GaSb wetting layer (WL) – approximately 1 nm, in agreement with previous works [39,40] –, a defining characteristic of the Stranski-Krastanov growth mode. Further details of the structural properties of GaSb/GaAs QDs grown under these conditions are described in Ref. [41].

B. Study of the light-intensity dependence in two-photon processes in IBSCs and OTIPs
1. Type-II hole-based IBSC.

IBSCs can potentially achieve 63% conversion efficiency [2]. To achieve this, one key operating principle is the production of two-photon sub-bandgap photocurrent as a consequence of process (I). In Ref. [36] we reported spectrally resolved two-photon photocurrent (process (I)) in our GaSb/GaAs QDs. In Figure 4a, we extend those results by further increasing the light intensity of the photon flux. Details of the experimental set-up can be found in Refs. [7] and [36], and in the Samples and Methods Section. The general principle is that the sample can be simultaneously illuminated by two monochromatic light beams identified as ph1 and ph2. The energy of photons from ph1, E_{ph1}, can be tuned between 0.2 and 1.9 eV. The energy of photons from ph2, E_{ph2}, is kept constant. In these measurements, signal response to ph1 is monitored via lock-in techniques, while ph2 sets the steady-state biasing conditions of the measurement. Samples are measured under short-circuit conditions; i.e., no electrical power is supplied to the device under test.

In order to study process (I), we have chosen $E_{ph2} = 1.32$ eV, fulfilling the condition $E_H < E_{ph2} < E_G$. Figure 4a shows the results of the two-photon process (I) measurements at 9 K. The y-axis represents the quantum efficiency (QE) of our IBSC prototypes in response to ph1 illumination, whose energy is represented on the x-axis. The thick black line corresponds to the case of ph1-only illumination, QE_{1ph}. Three absorption thresholds can be identified, corresponding to E_G, E_H and E_L, indicated by the dashed lines in Figure 4a. The abrupt decrease near 1.52 eV closely matches the theoretical bandgap of GaAs, E_G, at 9 K. E_H, as defined in Figure 1b, is related to the transition of the ground state for holes in the QDs to the bottom of the CB. QE_{1ph} shows a smooth signature in the 1–1.1 eV range. Electroluminescence measurements of our samples more accurately reveal the value of E_H at approximately 1.02 eV, as shown in the inset of Figure 4b (see Ref. [36] for more detailed analysis of the electroluminescence spectrum). The measured E_H is within the range of prior reports (1.0–1.3 eV) [32,38,39,42,43], though in the low energy range. Sb-As intermixing and the shape of the dots may explain the variations of E_H [44]. The value of E_L –the confining energy of IB– is 0.49 ± 0.01 eV. This value was obtained in Ref. [36] from the process (I) photocurrent measurements and is reassured in this work by photocurrent measurements of process (II).

The method for accurately determining E_L will be described below. The semi-empirical calculation of E_L, presented in Section III.D, is also in agreement with our measurements. In our samples E_L is somewhat higher than values reported in previous reports [45,46] with one exception [44]. The high value of E_L is in agreement with the low value of E_H since both have to add up to E_G. Note that in our QDs, $E_L + E_H \approx 1.51 \pm 0.01$ eV $\approx E_G = 1.52$ eV, as expected for type-II QDs. The small difference between the measured $E_L + E_H$ and E_G may be due to rounding errors or the fact that the actual bandgap of the GaAs matrix in our devices could be lower due to bandgap narrowing related to heavy doping [47,48].
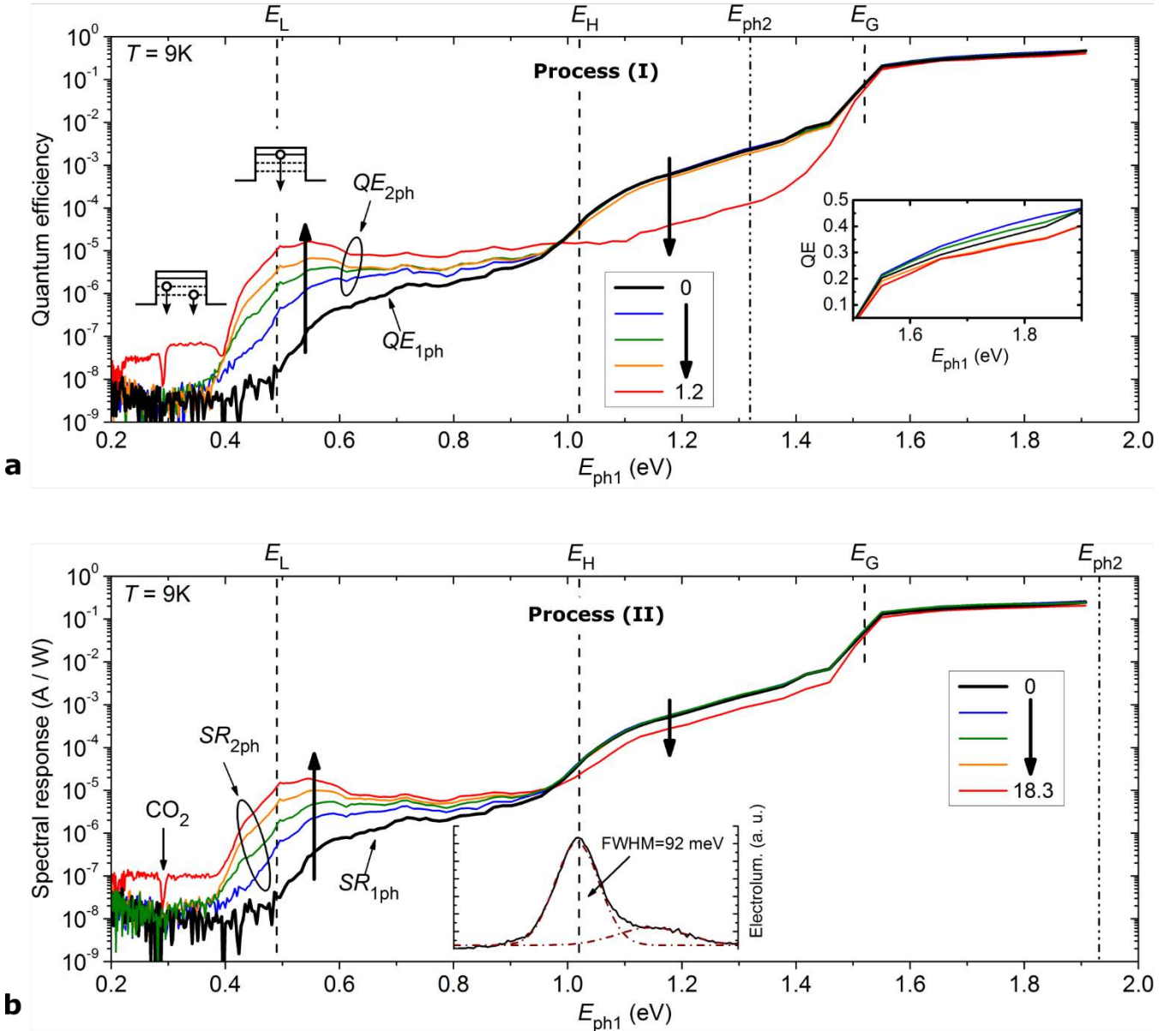

Figure 4. Two-photon process (I) and process (II) photocurrent measurements at 9K. The three absorption bandgaps, E_G, E_H and E_L are indicated. The thick black line corresponds to the ph1-only illumination case, QE_{1ph} (SR_{1ph}). The colored QE lines correspond to the two-photon illumination case, QE_{2ph} (SR_{2ph}), for different intensities of ph2. The legends indicate the approximate values of the employed ph2 intensities (in $\mu W/cm^2$). The thick black arrows indicate the anti-symmetrical behavior of the QE (SR). (a) Process (I). $E_{ph2} = 1.32$ eV. The right inset is a magnification in linear scale of the above-bandgap range of the measurements. The two left insets illustrate transitions from a hole in the ground state (solid line) and from excited states (dashed lines) in the potential well, at energies

$E = E_L$ and $E < E_L$, respectively. (b) Process (II). E_{ph2} = 1.93 eV. A CO_2 absorption line is indicated. The inset plots the measured electroluminescence of our samples, and its fitting to two gaussian functions.

Under ph1-only illumination, QE_{1ph} is in the 10^{-5}–10^{-2} range for $E_H < E_{ph1} < E_G$. In particular, $QE_{1ph}(E_H) \approx 5 \cdot 10^{-5}$. For $E_{ph1} < E_H$, QE_{1ph} diminishes until it merges with the noise level of the measurement. In particular, $QE_{1ph}(E_L)$ is approximately 10^{-8}. The low value of the sub-bandgap QE_{1ph} is explained by the lack of an efficient mechanism —under monochromatic sub-bandgap illumination— to complete the remaining second optical transition that would enable photocurrent. Let us now analyze the impact of varying ph2 intensity for different energy regions of the QE spectrum (coloured lines in Figure 4a, QE_{2ph}). For all of the employed intensities, the QE greatly increases with the addition of ph2 in the energy range near E_L. This result indicates that the two-photon process (I) takes place in our hole-based IBSC. When photons from the ph2 beam are absorbed, holes are created in the IB, enabling the absorption of photons from the ph1 beam and the generation of a measurable external photocurrent. The QE trend is, however, very different for $E_H < E_{ph1} < E_G$. Under the lowest ph2 intensities (blue, green and orange lines), QE_{2ph} remains constant or is slightly reduced. However, under "high" ph2 intensities (red line), QE_{2ph} is drastically reduced. At this point, a remarkable behavior must be highlighted: under the highest ph2 intensity (red line), finite QE is also measured for $E_{ph1} < E_L$ in the 0.2–0.4 eV range. At these energies, the measured QE_{2ph} is in the 10^{-8}–10^{-7} range. As discussed in Section III.E, absorption for $E < E_L$ involves transitions of holes from confined excited states in the potential well. Such transitions are illustrated in the left inset of Figure 4a. This anti-symmetrical behavior of the QE (increase for $E < E_H$, decrease for $E_H < E < E_G$) will be discussed in Section III.E. Finally, the inset of Figure 4a shows the evolution of the QE with ph2 intensity for $E > E_G$ (notice that the plot is in linear scale). For this energy range, the QE results change only slightly, with no clear dependence with the intensity of ph2.

Although in our measurements we could not clearly identify electronic transitions related to the WL, it cannot be precluded that photons with $E = E_{ph2}$ = 1.32 eV may be absorbed in the WL. Previous works have reported energy values for transitions related to the WL in GaSb/GaAs QDs both lower [39,42] and higher [41,46] than E_{ph2}. In any case, the net effect of photon absorption in the WL would result in the population of the IB with holes, as a consequence of fast carrier thermalization and transfer from the WL to the QDs [49].

2. Type-II hole-based OTIP.

OTIPs have two differentiating features [7]: (1) they can be optically switched ON/OFF as a consequence of two-photon process (II), and (2) they do not need an external DC bias to operate. In order to verify the occurrence of process (II) in our samples, we have repeated the two-photon experiments previously analyzed, with the modification that the energy of photons from ph2 has been chosen to be above the bandgap; specifically, E_{ph2}=1.93 eV. The results are shown in Figure 4b. The y-axis represents the spectral response (SR) of our devices, expressed as responsivity in units of A/W. The thick black line corresponds to the ph1-only illumination case, SR_{1ph}, and the colored lines to the two-photon illumination case, SR_{2ph}. The response at energies close to E_L clearly increases with the addition of ph2. $SR_{1ph}(E_L)$ cannot be accurately determined since it is near the noise level of our measurements (we recall this is aligned with the IBSC theory since response to sub-bandgap illumination at a single energy should be negligible). In contrast, $SR_{2ph}(E_L) \approx 10^{-5}$ A/W for the highest intensity of ph2 (red line), which demonstrate optically-triggered detection in our samples. In Ref. [7] the maximum temperature at which OTIP operation was demonstrated for electron-based OTIPs was 60 K. Here we demonstrate OTIP operation at temperatures as high as 200 K (Supplemental Material, Figure S2). We ascribe this surprising result to the low background detection noise of our device.
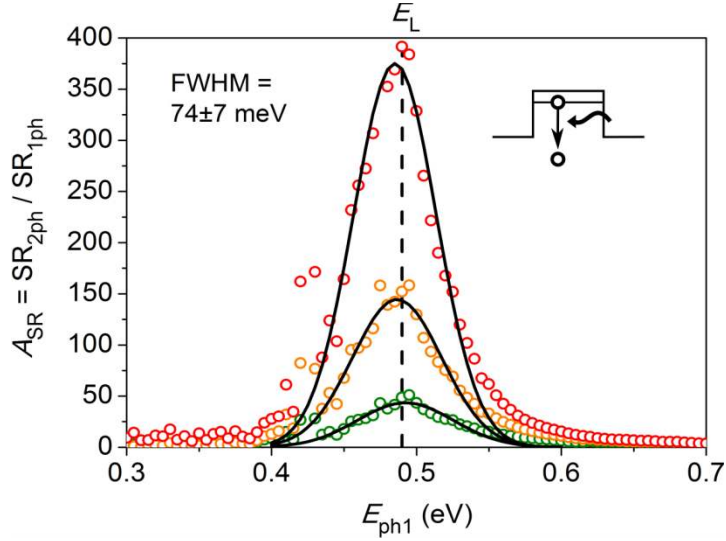
8

Figure 5. A_{SR} measured in our hole-based OTIP for different intensities of ph2 ($E_{ph2} = 1.93eV$). Measured data are represented by circles, Gaussian fittings by solid lines. The dashed line indicates the fitted value of E_L. The inset illustrates the E_L–related hole transition.

Similar to the QE case, the impact of ph2 on the SR of our samples is energy dependent. We define $A_{SR}(E) = SR_{2ph}(E)/SR_{1ph}(E)$ as *amplification in spectral response*. By calculating A_{SR} one can identify the ph1 energies that contribute the most to two-photon process (II). This is represented in Figure 5, where $A_{SR}(E)$ is plotted for three intensity values of ph2. The measured data are represented with open circles. The curves are well described by Gaussian functions centered at 0.49 ± 0.01 eV. This value is similar to the result in Ref. [36] after photocurrent measurements related to process (I). We believe that this value corresponds to E_L as illustrated in Figure 1b. In other words, A_{SR} reveals the absorption spectrum related to the confined holes in the GaSb QDs, which peaks at the IB→VB transition energy. In fact, the fitted value of E_L is red-shifted with increasing intensity of ph2, ranging from 498 meV at the lowest intensity to 485 meV at the highest intensity. This result is in agreement with the reported blue-shift of E_H under strong illumination [38,39,42,43]. The non-zero width of the E_H-related emission is usually attributed to inhomogeneity in the QD size and shape. Since $E_G \approx E_H + E_L$ in our type-II QDs, it follows that an increase/decrease in E_H should be accompanied by a similar decrease/increase in E_L; hence, the full width at half maximum (FWHM) of the two measured parameters should be similar. The FWHM of the Gaussian fittings of A_{SR} is 74 ± 7 meV, which is close to that of the E_H emission spectrum (≈ 92 meV, Figure 4b). These data further support that A_{SR} reveals E_L. As previously observed in the process (I) results, an anti-symmetrical behavior is observed: SR_{2ph} increases at high ph2 intensity for $E_{ph1} < E_H$, while SR_{2ph} decreases at high ph2 intensity for $E_H < E_{ph1} < E_G$. Again, for the highest employed intensity of ph2 (red line in Figure 4b), absorption for energies lower than E_L (0.2–0.4 eV) is detected, which indicates the participation of excited holes (in the QD potential well) in the absorption processes.

The fitted value of A_{SR} at E_L has a logarithmic dependence with ph2 intensity, F_{ph2}, as shown in the Supplemental Material (Figure S3). For the highest intensity, A_{SR} is almost 400, which means that the response to IR light in our hole-based OTIP has been increased by more than two orders of magnitude due to ph2 triggering. The optical-switching performance of our device greatly exceeds that of the first reported prototype based on InAs/AlGaAs QDs [7], for which A_{SR} was around 6. However, this performance enhancement is not due to a higher responsivity. Actually, the

OTIP of Ref. [7] exhibited a maximum $SR_{2ph}(E_L) \approx 10^{-4}$ A/W, while it is only $\approx 10^{-5}$ A/W in our hole-based device. Hence, it is the low value of $SR_{1ph}(E_L)$ that is advantageous by providing a low background OFF mode for the OTIP and, consequently, a higher value for A_{SR}. A_{SR} also provides an indication of the signal-to-noise ratio for optical detection.

C. Demonstration of two-photon photovoltage

The second pillar of the high conversion efficiency potential of IBSCs is *voltage preservation*. This states that the extra recombination introduced by the IB does not limit the output voltage of the devices [2]. In other words, although below-bandgap photons participate in the generation of photocurrent, the output voltage of the device can exceed the absorption threshold energy (divided by the electron charge, e) and is only limited by the bandgap E_G. In an IB material out of equilibrium, the presence of three distinct electronic bands justifies the use of three distinct quasi-Fermi levels (chemical potentials) for the respective electronic populations: E_{Fe} for the CB, E_{Fh} for the VB, and E_{FIB} for the IB (see Figure 6). Conversely, in the selective contacts (p and n semiconductors, in our case, see Figure S1 in the Supplemental Material), only two quasi-Fermi levels (E_{Fe} and E_{Fh}) apply. The electron-hole pairs generated in the IB material via process (I) can be extracted through the selective contacts at a voltage $V = (E_{Fe} - E_{Fh})/e$, and, therefore with the possibility of exceeding E_H/e.
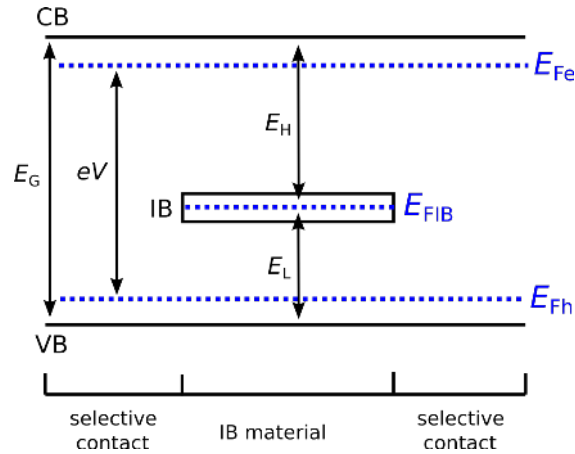

Figure 6. Quasi-Fermi levels and voltage preservation in an IBSC.

Voltage preservation has been demonstrated in electron-based devices under white-light or monochromatic, above-bandgap illumination [10,28,50]. In fact, $E_{Fe} - E_{Fh}$ can only approach E_G if non-equilibrium between the IB and the conduction and valence bands can be sustained [51]. This means that carrier generation through the absorption of external photons must be stronger than thermal generation, which is not usually the case in QD-IBSC prototypes working at room temperature [25,51]. For this reason, in the aforementioned works, voltage preservation could only be demonstrated at low temperatures.

The direct demonstration of the effective contribution of sub-bandgap two-photon absorption to the generation of output voltage has remained elusive. With that aim, we have performed *two-photon photovoltage* measurements in our GaSb/GaAs samples. The results at 9K are shown in Figure 7. The sample is illuminated with two monochromatic light beams, just as in the case of the two-photon results of Figure 4a. E_{ph2}=1.32 eV while E_{ph1} is swept from 0.2 to 1.9 eV. The intensity of ph2 is constant during one measurement but changed for each new measurement. The y-axis plots the

measured increase in V_{OC} when both light beams are illuminating the sample. It is important to remark that, because the measurement is locked to ph1 excitation, the measured photovoltage is the variation in V_{OC}, ΔV_{OC}, due to the addition of ph1 with respect to the steady-state V_{OC}, $V_{OC,SS}$, that is, the value induced by the continuous-wave ph2 illumination.
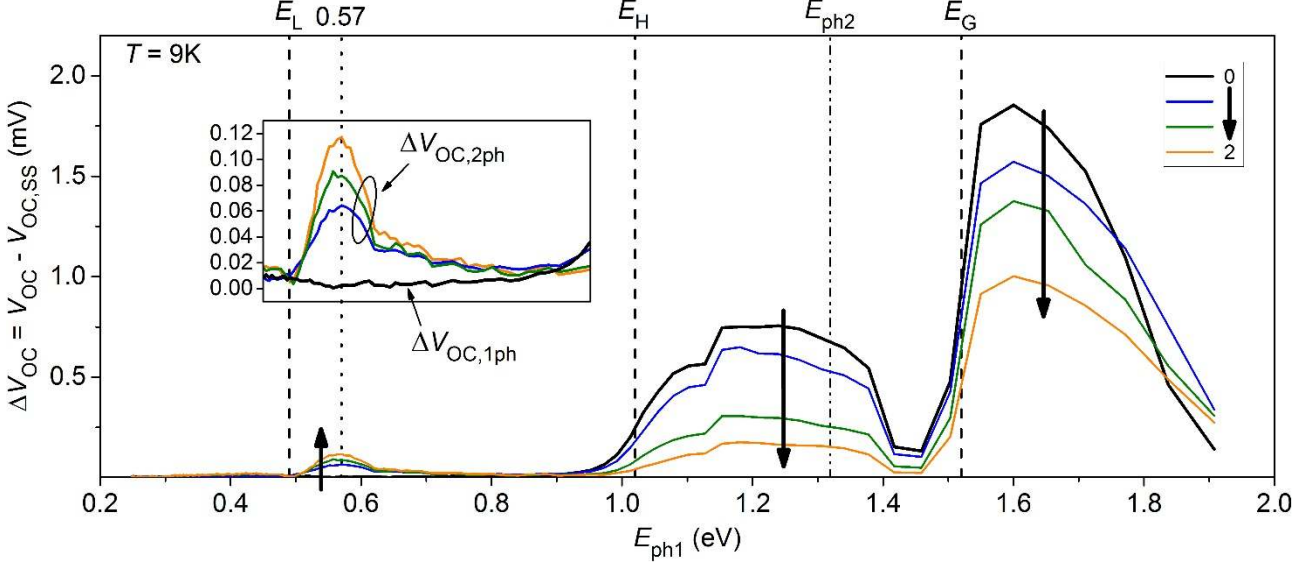

Figure 7. Two-photon photovoltage measurements at 9K. The three absorption bandgaps, E_G, E_H and E_L are indicated with dashed lines. E_{ph2} = 1.32 eV is also indicated. The thick black line corresponds to the ph1-only illumination case, $\Delta V_{OC,1ph}$. The colored lines correspond to the two-photon illumination case, $\Delta V_{OC,2ph}$, for different intensities of ph2. The legend indicates the approximated values of $V_{OC,SS}$ (in mV) for the different intensities of ph2. The thick black arrows indicate the anti-symmetrical behavior of ΔV_{OC}. The inset is a magnification of the $E_L < E < E_H$ range of the measurement.

Before analyzing the results, we would like to highlight the fact that we have used a SiC IR lamp as photon source for ph1. The blackbody emission of this source peaks at around 0.4 eV and decays rapidly for higher energies. The thick black line represents the measurement in which ph2 is kept OFF; i. e., ph1-only illumination is used ($\Delta V_{OC,1ph}$). Note that $\Delta V_{OC,1ph}$ equals the actual value of V_{OC}, because $V_{OC,SS} = 0$. Let us analyze for that case the three energy ranges of interest. For $E > E_G$, ΔV_{OC} is greater than zero, peaking at around 1.5 mV. Note that, in the high energy range, ΔV_{OC} decreases following the reduction in photon flux coming from the IR source. For $E_G > E > E_H$, ΔV_{OC} is in the 0.5–0.8 mV range. The abrupt fall in $\Delta V_{OC,1ph}$ for energies just below E_G is due to the strong reduction in absorptivity (and hence in photo-generated carriers) in the GaSb QDs as compared to the GaAs bulk (as it is shown in the QE results of Figure 4a). $\Delta V_{OC,1ph}$ increases again for lower energy values following the recovery in the photon flux intensity. Below 1.1 eV photon illumination, $\Delta V_{OC,1ph}$ decays rapidly again, following the rapid decrease in QE_{1ph}, and finally goes to zero for $E < E_H$. As expected, the spectral $\Delta V_{OC,1ph}$ is consistent with the product of the QE_{1ph} and the flux intensity (IR source). In our measurements, this product always results in very low values of photo-generated carriers (the measured current densities are in the nA/cm^2 range), which in turn explain why the values measured of $\Delta V_{OC,1ph}$ are in the mV range.

With the addition of ph2, two-photon ΔV_{OC} ($\Delta V_{OC,2ph}$) is measured for $E_L < E < E_H$. In this range, ΔV_{OC} increases with the intensity of ph2. These results demonstrate an increase in V_{OC} of our GaSb/GaAs samples resulting from two-photon sub-bandgap illumination. We call this phenomenon *two-photon photovoltage*. Furthermore, our measurements spectrally resolve which photon energies contribute more efficiently to it. For $E > E_H$, ΔV_{OC} decreases with increasing ph2 intensity. The $\Delta V_{OC,2ph}$ decrease for $E_H < E < E_G$ is consistent with the QE_{2ph} reduction observed in Figure 4a for the

11

highest ph2 intensity. On the contrary, the $\Delta V_{OC,2ph}$ decrease for $E > E_G$ does not seem to correlate to the QE_{2ph} results, where QE_{2ph} is shown not to have an apparent dependence on ph2 (right inset, Figure 4a). In reality, $V_{OC,2ph}$ and QE_{2ph} are both consistent, as explained in the following. Our results show $\Delta V_{OC,2ph} = V_{OC,2ph} - V_{OC,SS}$, where $V_{OC,2ph}$ is the total open-circuit voltage under two-photon illumination. It is straightforward to derive from Shockley's diode equation that

$$\Delta V_{OC,2ph} = kT/e \ \ln\left(I_{L,2ph}/I_{L,SS}\right) \quad (1)$$

(for $I_{L,2ph} \gg I_0$ and $I_{L,SS} \gg I_0$), where k is the Boltzmann constant, T the temperature, $I_{L,2ph}$ and $I_{L,SS}$ are the photo-generated currents under two-photon illumination and steady-state-only (ph2) illumination, respectively, and I is the reverse saturation current of the diode. If we define $\Delta I = I_{L,2ph} - I_{L,SS}$, then

$$\Delta V_{OC,2ph} = kT/e \ \ln\left[1 + \left(\Delta I/I_{L,SS}\right)\right] \quad (2)$$

From Equation (2), for a constant ΔI, $\Delta V_{OC,2ph}$ will decrease if $I_{L,SS}$ increases. The results in Figure 4a show that QE_{2ph} is roughly constant with ph2 illumination for $E > E_G$. In the case of Equation (2), this will result in constant ΔI. However, an increase in ph2 implies an increase in the steady-state current flowing through the device, implying an increase in $I_{L,SS}$. Therefore, $\Delta V_{OC,2ph}$ is expected to be reduced with an increasing intensity of ph2, even if QE_{2ph} remains constant. In fact, the increase in $V_{OC,SS}$ as $I_{L,SS}$ increases should also impact $\Delta V_{OC,2ph}$ for $E < E_G$, which means that part of the ΔV_{OC} decrease in the $E_H < E < E_G$ range is not due to the reduction in ΔI (reduction in QE_{2ph}), but to the increase in $I_{L,SS}$ that follows ph2 intensity.

Finally, we analyze the shape of the $\Delta V_{OC,2ph}$ spectra in the $E_L < E < E_H$ range (inset of Figure 7). It resembles that of the QE_{2ph} except for the fact that $\Delta V_{OC,2ph}$ goes close to zero for $E = E_L$. Gaussian fittings of $\Delta V_{OC,2ph}$ (shown in the Supplemental Material, Figure S4) indicate a strong contribution to the photovoltage at $E = 0.57$ eV, and marginal contribution for lower energies. We attribute this result to strong hole absorption between a confined state in the QDs and a resonant state in the VB of the host [52]. It seems that, even if absorption at E_L is efficient in the production of two-photon photocurrent, it is not efficient in the generation of a photovoltage. The reasons for this are currently unclear. One possibility is that under increasing positive voltage bias of the device (V_{OC}), relaxation of excited holes back into the QD becomes faster than carrier extraction. In fact, carrier relaxation is known to be very fast in the well-studied type-I InAs/GaAs system [49,53,54]. We believe that a blue-shift of E_L due to the quantum-confined Stark effect [55] under illumination is unlikely because: (1) for all ph2 intensities the fitted ΔV_{OC} peaks at the same energy (Supplemental Material, Figure S4), and (2) the reduction of the internal electric field due to ph1 illumination (smaller than 25 V/cm, see the Supplemental Material) is too low to cause such a high energy shift (80 meV) [56].

D. Theoretical modeling of the GaSb/GaAs QD energy structure

In Section III.B we have given experimental evidence of the bandgap distribution of our GaSb/GaAs QDs at 9K: E_G=1.52 eV, E_H=1.02 eV and $E_L \approx 0.49$ eV. This bandgap distribution directly results from the type-II confinement of the GaSb QDs and the fact that the IB is located 0.49 eV above the VB of the GaAs. Now we will further support these results by comparing them with theoretical calculations. We have employed the method described in Refs. [57] and [58]. This method provides a means to obtain the carrier energy states in arbitrary-shaped QDs within the framework of the effective mass model. In Figure 3c, a cross section of a truncated pyramid (a trapezoid) is superimposed with a TEM image of one of the QDs, indicating that the QD shape corresponds to a truncated pyramid with symmetry defined by

the C_{nv} group. The symmetry used for defining the shape of the QD allows also classifying the symmetry of the carrier envelope wavefunction accordingly to the irreducible representations of the C_{nv} group. In our analysis, we have used truncated pyramids with $n=30$, 50 vertices and with a height $h = (1 - p) \cdot h_0$, where h_0 is the height of the original non-truncated pyramid and p is the truncating factor. d is the base diameter of the truncated pyramid. This method enables us to calculate and identify the energy of the confined levels in the QD potential well for a given set of values $\{d, h, p\}$. According to the size estimation from TEM images (such as those shown in Figure 3) we have explored QDs characterized by 9.0 nm $\leq d \leq$ 11.0 nm, 3.0 nm $\leq h \leq$ 4.0 nm, and $p=0$, 0.5 and 0.7. Input parameters are the electron effective masses in the well, $m_{w,e} = 0.060\ m_0$ [59], and in the barrier, $m_{b,e} = 0.067\ m_0$ [60]; hole effective masses in the well, $m_{w,h} = 0.097\ m_0$ [59], and in the barrier, $m_{b,h} = 0.377\ m_0$ [61]; and height of the potential well in the VB, $V_h = 0.57$ eV [62,63], where m_0 is the free electron mass.
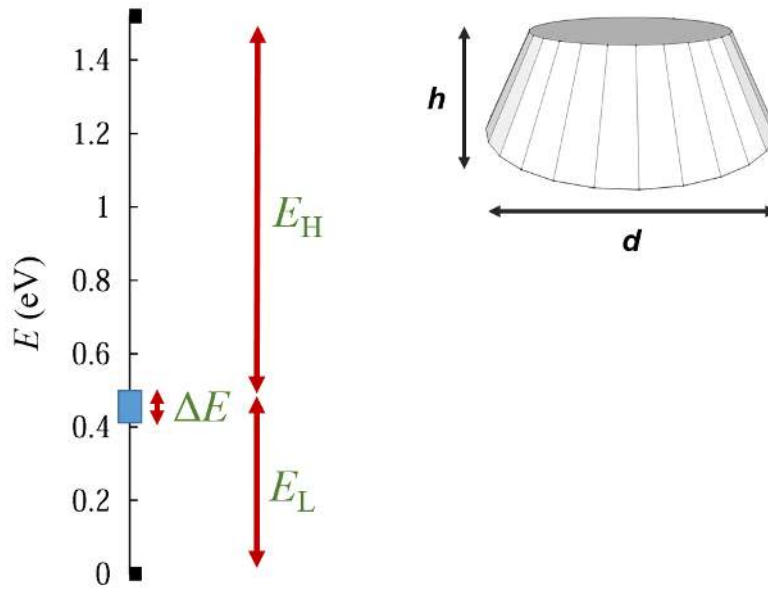

Figure 8. Calculated energy band diagram of the GaSb/GaAs QDs. The axis represents electron energy, with the origin in the edge of the GaAs VB. The blue area ΔE represents the dispersion of the calculated hole ground state energy for the different employed values of the geometrical parameters. The QD geometry used in the calculations is sketched in the upper-right part of the figure.

Figure 8 depicts the results of our calculations. The height of the blue rectangle, ΔE, represents the dispersion of the values obtained for E_L. Note that without any fitting, the value of E_L is in the 0.4–0.5 eV range, in agreement with experiments. Hence, our calculations support the conclusion that experimentally measured absorption at 0.49 eV is linked to the E_L bandgap. For the values explored, h is the parameter with strongest impact on ΔE. For example, for $h = 4$ nm and $p \geq 0.5$, $E_L \approx 0.49$ eV for all the values of d. A large number of confined holes states (not shown in Figure 8) appear below the ground state. To provide an idea of the density of states, for the set of geometrical parameters $\{d, h, p\}=\{10$ nm, 4 nm, 0.7$\}$, there are 100 confined states in the 0.486–0.183 eV interval. The presence of these excited states supports the possibility of photon absorption with $E < E_L$, as shown in Figure 4a and b, and discussed in Section III.E.

E. Intermediate-band absorption theory framework

The QE_{2ph}, SR_{2ph}, and $\Delta V_{OC,2ph}$ results presented in this work reveal opposing dependency of absorption related to E_H and E_L on light bias intensity. We will now analyze this phenomenon focusing on process (I) measured in Figure 4a, where a similar analysis can be carried out for process (II). For low values of F_{ph2}, QE_{2ph} increases for $E_{ph1} < E_H$ and remains roughly constant for $E_H < E_{ph1} < E_G$. For high values of F_{ph2}, QE_{2ph} keeps increasing for $E_{ph1} < E_H$—even finite QE_{2ph} is measured for $E_{ph1} < E_L$— but decreases abruptly for $E_H < E_{ph1} < E_G$. An explanation for this behavior is shown in the energy band diagrams of Figure 9, illustrating absorption mechanisms for a single QD including hole excited states. Figure 9a and Figure 9b illustrate the cases for "low" and "high" values of F_{ph2}, respectively. It is important to recall that the IB framework describes the electronic population of each band through its own quasi-Fermi level (Figure 6). In Figure 9, E_F is the Fermi level in equilibrium.
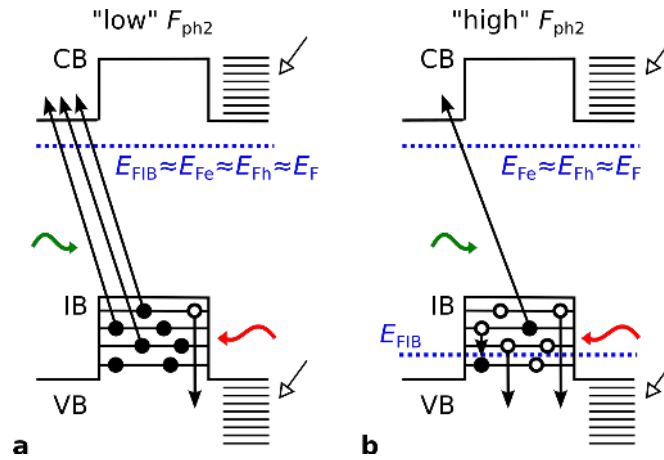

Figure 9. Simplified energy band diagram of a QD and quasi-Fermi levels in hole-based IB devices for (a) "low" values of F_{ph2}, and (b) "high" values of F_{ph2}. The high density of states of the VB and the CB is represented by the closely-spaced horizontal bars (indicated by open arrows). For each case, the electron (filled black circles) and hole (open circles) populations of the IB are indicated. The green and red arrows indicate photons from ph1 with different energies (green, $E_H < E_{ph1} < E_G$, and red, $E_{ph1} < E_H$). Black arrows represent electron (hole) transitions from the IB to the CB (VB) after ph1 absorption.

The QD-stack of our devices is placed in an n-type (10^{16}–10^{17} cm^{-3}) region (see Supplemental Material, Figure S1). In that region, E_F is near the bottom edge of the CB, since GaSb QDs do not introduce empty levels below the CB to accept electrons. The confined hole states of the QDs, which are less than 0.5 eV above the VB of the GaAs, are occupied by electrons. Excitation of ph2 promotes electrons from the IB to the CB and therefore only impacts the populations of the IB and the CB. Under low F_{ph2}, the populations of those two bands have not been significantly modified, hence, $E_{FIB} \approx E_{Fe} \approx E_{Fh} \approx E_F$. We can relate the low and high excitation conditions directly to the density of states (DOS) of the IB (approximately 5×10^{15} cm^{-3}). The high DOS of the VB and the CB is represented in Figure 9 by closely spaced horizontal bars. We will define *low* F_{ph2} as the condition that does not significantly alter the population of the IB, and *high* F_{ph2} as the condition that significantly alters the population of the IB. Hence, the quantitative value of the transition between low and high excitation will depend on the DOS of the IB.

Under low F_{ph2}, the IB is nearly filled with electrons. This explains that, when sweeping the energy of ph1, high absorption is observed for $E_H < E_{ph1} < E_G$ and low absorption for $E_{ph1} < E_H$, since there are few holes available to absorb the low-energy IR photons. As F_{ph2} increases, fewer electrons occupy the IB, corresponding to an increasing population by holes. This, in turn, results in an increased QE_{2ph} due to the availability of holes to allow the absorption of

low-energy IR photons. For high values of F_{ph2}, the IB is nearly filled with holes (depleted of electrons), leading to a decrease in QE_{2ph} for $E_H < E_{ph1} < E_G$ due to a lack of electrons available for promotion to the CB. Simultaneously, since the excited confined states are populated with holes, absorption for $E_{ph1} < E_L$ is enabled – holes are promoted from an excited state to a higher excited state or to a resonant state in the VB of the GaAs – and QE_{2ph} response is observed. Although this analysis has been carried out for hole-based IB, a similar behavior is expected for an IB with confinement of electrons.

To validate this analysis, we have modeled the variation in E_{FIB} that is induced by ph2 and that causes the measured anti-symmetrical increase/decrease in the SR at E_H and E_L (Figure 4b). The model is based on the following assumptions: (1) The SR is directly proportional to photon absorption, and that this proportionality is invariant in the conditions of our measurements. (2) E_{Fe} and E_{Fh} are unperturbed by ph2. (3) For a particular photon energy, the absorptivity of the QDs is proportional to the population of electrons (or holes) in the IB, and does not depend on any other parameter. (4) Non-overlap of absorption coefficients is assumed, which means that the absorption of a photon with energy E_H will primarily result in the excitation of an electron from the IB to the CB, and not the excitation of a hole from the IB to the VB. (5) For simplicity, a narrow IB with all the energy levels mainly located at the hole ground state energy, E_{IB} (0.49 eV above the VB).

We define f_e as the electron-filling factor of the IB ($0 \leq f_e \leq 1$). Therefore, $f_h = (1 - f_e)$ is the hole filling factor of the IB. From the Fermi-Dirac distribution, we know that the probability, f, that an electronic level with energy E is occupied is:

$$f(E, E_F) = \frac{1}{1+\exp\left[(E-E_F)/_{kT}\right]} \quad (3)$$

Specifying Equation (3) for the case of the IB out of the equilibrium, we obtain Equation (4):

$$f_e(E_{FIB}) = \frac{1}{1+\exp\left[(E_{IB}-E_{FIB})/_{kT}\right]} \quad (4)$$

From assumptions (1–5), we deduce that SR is proportional to f_e and f_h. In particular, $SR_{2ph}(E_H) \propto f_e$ and $SR_{2ph}(E_L) \propto f_h$. We want to prove that ph2 modulates the position of E_{FIB}, and that this modulation, in turn, explains the photocurrent results. Therefore, for the SR measurements, we define $E_{FIB,0}$ as the position of the quasi-Fermi level of the IB under the lowest intensity of ph2 employed, $F_{ph2,0}$. As F_{ph2} increases, E_{FIB} shifts by ΔE_{FIB}, so that

$$E_{FIB}(F_{ph2}) = E_{FIB,0} + \Delta E_{FIB}(F_{ph2}) \quad (5)$$

Then:

$$R_{E_H}(F_{ph2}) = \frac{SR_{2ph}(E_H, F_{ph2})}{SR_{2ph}(E_H, F_{ph2,0})} = \frac{f_e(F_{ph2})}{f_e(F_{ph2,0})} = \frac{1+\exp\left[(E_{IB}-E_{FIB,0})/_{kT}\right]}{1+\exp\left[(E_{IB}-E_{FIB,0}-\Delta E_{FIB}(F_{ph2}))/_{kT}\right]} \quad (6)$$

where $R_{E_H}(F_{ph2})$ is the increment in SR_{2ph} at E_H caused by the increment in F_{ph2} with respect to $F_{ph2,0}$. Similarly,

$$R_{E_L}(F_{ph2}) = \frac{SR_{2ph}(E_L, F_{ph2})}{SR_{2ph}(E_L, F_{ph2,0})} = \frac{f_h(F_{ph2})}{f_h(F_{ph2,0})} = \frac{\exp\left[(E_{IB}-E_{FIB,0}-\Delta E_{FIB}(F_{ph2}))/_{kT}\right]*\left(1+\exp\left[(E_{IB}-E_{FIB,0})/_{kT}\right]\right)}{\exp\left[(E_{IB}-E_{FIB,0})/_{kT}\right]*\left(1+\exp\left[(E_{IB}-E_{FIB,0}-\Delta E_{FIB}(F_{ph2}))/_{kT}\right]\right)} \quad (7)$$

where $R_{E_L}(F_{ph2})$ is the increment in SR_{2ph} at E_L caused by the increment in F_{ph2} with respect to $F_{ph2,0}$. Formulas (6) and (7) also apply to the QE measurements, simply by replacing SR by QE. We have calculated the experimental values of R_{E_H} and R_{E_L} for all the ph2 intensities employed in our measurements and fitted the parameter $\Delta E_0 = E_{IB} - E_{FIB,0}$ in equations (6) and (7) in order to obtain the minimum square error for $\Delta E_{FIB}(F_{ph2})$. For each value of F_{ph2}, the error, x, was defined as

$$x(F_{ph2}) = \left| \frac{\Delta E_{FIB}(F_{ph2})|_{E_H} - \Delta E_{FIB}(F_{ph2})|_{E_L}}{\frac{1}{2}\left(\Delta E_{FIB}(F_{ph2})|_{E_H} + \Delta E_{FIB}(F_{ph2})|_{E_L}\right)} \right| \quad (8)$$

where $\Delta E_{FIB}|_{E_H}$ is the shift in E_{FIB} obtained from Equation (6), and $\Delta E_{FIB}|_{E_L}$ is the shift in E_{FIB} obtained from Equation (7). If the model explains the experiments, the shifts in E_{FIB} which explain the measured values of $SR_{2ph}(E_H)$ should also explain the measured values of $SR_{2ph}(E_L)$ and vice versa.

Figure 10 shows the results of our model. Black triangles represents $\Delta E_{FIB}|_{E_H}$ while red circles represent $\Delta E_{FIB}|_{E_L}$. The shadowed area represents the range in which ΔE_{FIB} values varies assuming an error of $\pm5\%$ in the measurements of R_{E_H} and R_{E_L}. The numeric values close to the triangles and circles are, respectively, the measured values of R_{E_H} and R_{E_L} which have been used for obtaining ΔE_{FIB}. The value of ΔE_0 which led to the smallest x is -3.1 meV. This means that, under the lowest employed F_{ph2} (0.11 μW/cm^2), E_{FIB} is 3.1 meV above the IB. At $T = 9$ K, this corresponds to $f_e =$ 0.98. Note that, at such low temperatures, the Fermi-Dirac distribution changes abruptly from almost 0 to almost 1 in only a few meV around E_F (see Supplemental Material, Figure S5). The close-to-1 value of f_e means that, under those conditions, the IB is practically filled with electrons, which results in "high" absorptivity for photon energies around E_H and "low" absorptivity for E_L, and hence the corresponding "high" and "low" values of $SR_{2ph}(E_H)$ and $SR_{2ph}(E_L)$ that have been measured, respectively.
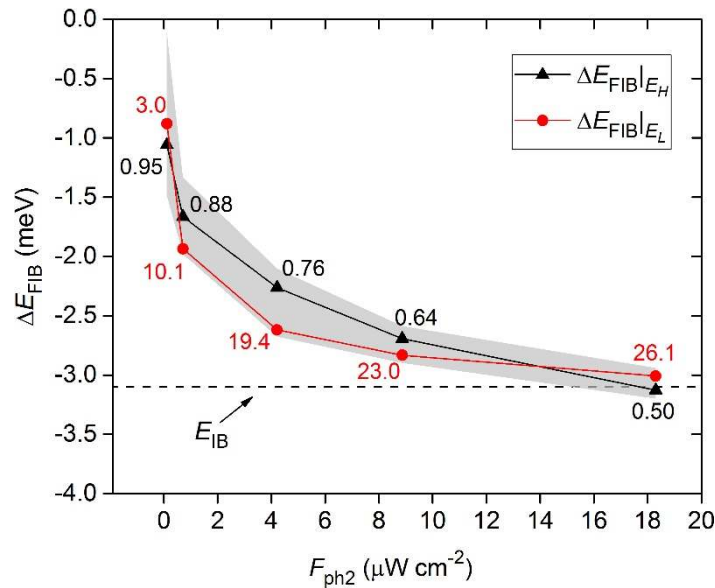

Figure 10. Evolution of ΔE_{FIB} as a function of F_{ph2} calculated from: Equation (6) (black triangles) and Equation (7) (red circles). The shadowed area represents the range in which the modeled ΔE_{FIB} values vary assuming an error of $\pm5\%$ in the measurements of R_{E_H} and R_{E_L}. The numeric values close to the triangles and circles are, respectively, the measured values of R_{E_H} and R_{E_L} which have been used for obtaining ΔE_{FIB}. The dashed line represents the position the IB.

16

The shape and values of the modeled $\Delta E_{FIB}|_{E_H}$ and $\Delta E_{FIB}|_{E_L}$ are quite similar (the differences are in the few tenths of meV range), which means that our model explains well the experimental results. As F_{ph2} is increased, E_{FIB} shifts closer to the IB, thereby reducing f_e and increasing f_h. For the highest employed F_{ph2}, E_{FIB} falls approximately onto E_{IB}, which results in $f_e \approx f_h \approx 0.5$. This explains both that $SR_{2ph}(E_H)$ reduces by a factor 2 and $SR_{2ph}(E_L)$ increases by a factor 26.1.

Our results confirm that, as expected, sub-bandgap absorption in IB materials depends on the electronic filling of the IB. The fact that the QDs in our samples are emptied of holes under equilibrium conditions –due to their placement in an n-type region– explains the very low absorptivity at E_L under monochromatic illumination. This, in turn, is the cause of the low measured SR_{1ph} and good optical switching (ON/OFF) performance of our hole-based OTIPs. We conclude that, from the perspective of maximizing A_{SR}, OTIPs should be designed as to have an emptied IB under equilibrium conditions. However, it is possible that the responsivity of these devices – still too low for practical applications – be increased by partially filling the IB. In contrast, the IB in IBSCs should be half-filled [64] because strong absorption at both E_L and E_H is desired. The low light intensities employed in our experiments were enough to alter the population of the IB because of the low DOS of the IB. In order to achieve practical devices, the responsivity of OTIPs and the sub-bandgap QE of IBSCs should be boosted, and, for this, the DOS of the IB, and therefore, the volumetric density of the QDs, need to be increased. In addition, light management techniques could be used to enhance the absorptivity of sub-bandgap transitions [65,66].

Conclusion

We have studied the intermediate-band absorption properties of GaSb/GaAs QD IB devices (IBSC and OTIP). The experimental results are consistent with a type-II band diagram and an IB located 0.49 eV above the VB. The two-photon absorption processes, enabled by the presence of the IB, contribute to the generation of photocurrent and photovoltage. By means of light intensity-dependent two-photon experiments, we have demonstrated that the absorption strength of the VB to IB and IB to CB transitions are interrelated via the filling state of the IB. We have successfully modeled the interrelation between the VB➔IB and the IB➔CB absorptivities on the basis of the filling factor of the IB. In our devices the IB is depleted of holes under equilibrium conditions, which results in high absorptivity in transitions related to E_H and low absorptivity in transitions related to E_L. The hole-based IB can be filled directly by IB➔CB optical pumping of electrons or indirectly by VB➔CB optical pumping of electrons followed by VB➔IB hole relaxation. Photo-filling the IB produces an anti-symmetrical effect in the absorption properties of the material: absorptivity for E_L is enhanced while absorptivity for E_H is reduced. Under high photo-filling conditions, sub E_L transitions involving shallow confined states can be resolved. This work emphasizes the importance of engineering not only the IB energy but also its carrier population, depending on the intended device application. The IB in an IBSC should be ideally half-filled, so that both transitions from and to the IB can take place. In the hole-based OTIP, on the contrary, the initially emptied IB has proven beneficial to increase detection as a result from a reduced background dark current.

Acknowledgements

References

[1] M.A. Green and S.P. Bremner, Nat. Mater. **16**, 23 (2017).

[2] A. Luque and A. Martí, Phys. Rev. Lett. **78**, 5014 (1997).

[3] M. Wolf, Proc. IRE **48**, 1246 (1960).

[4] A. Luque, A. Martí, and C. Stanley, Nat. Photonics **6**, 146 (2012).

[5] I. Ramiro, A. Marti, E. Antolin, and A. Luque, IEEE J. Photovoltaics **4**, (2014).

[6] Y. Okada, N.J. Ekins-Daukes, T. Kita, R. Tamaki, M. Yoshida, A. Pusch, O. Hess, C.C. Phillips, D.J. Farrell, and K. Yoshida, Appl. Phys. Rev. **2**, 21302 (2015).

[7] Í. Ramiro, A. Martí, E. Antolín, E. López, A. Datas, A. Luque, J.M. Ripalda, and Y. González, Nano Lett. **15**, (2015).

[8] A. Martí, E. Antolín, C.R. Stanley, C.D. Farmer, N. Lopez, P. Díaz, E. Canovas, P.G. Linares, and A. Luque, Phys. Rev. Lett. **97**, 247701 (2006).

[9] A. Scaccabarozzi, S. Adorno, S. Bietti, M. Acciarri, and S. Sanguinetti, Phys. Status Solidi (RRL)-Rapid Res. Lett. **7**, 173 (2013).

[10] I. Ramiro, E. Antolin, P.G. Linares, E. Lopez, I. Artacho, A. Datas, A. Marti, A. Luque, M.J. Steer, and C.R. Stanley, in *2014 IEEE 40th Photovolt. Spec. Conf. PVSC 2014* (2014).

[11] R. Tamaki, Y. Shoji, Y. Okada, and K. Miyano, IEEE J. Photovoltaics **5**, 229 (2014).

[12] T. Nozawa, H. Takagi, K. Watanabe, and Y. Arakawa, Nano Lett. **15**, 4483 (2015).

[13] A. Martí, N. Lopez, E. Antolín, E. Canovas, A. Luque, C.R. Stanley, C.D. Farmer, and P. Díaz, Appl. Phys. Lett. **90**, 233510 (2007).

[14] R. Oshima, A. Takata, and Y. Okada, Appl. Phys. Lett. **93**, 83111 (2008).

[15] V. Popescu, G. Bester, M.C. Hanna, A.G. Norman, and A. Zunger, Phys. Rev. B **78**, 205317 (2008).

[16] R.B. Laghumavarapu, M. El-Emawy, N. Nuntawong, A. Moscho, L.F. Lester, and D.L. Huffaker, Appl. Phys. Lett. **91**, 243113 (2007).

[17] W.-S. Liu, H.-M. Wu, F.-H. Tsao, T.-L. Hsu, and J.-I. Chyi, Sol. Energy Mater. Sol. Cells **105**, 237 (2012).

[18] C.G. Bailey, D. V Forbes, R.P. Raffaelle, and S.M. Hubbard, Appl. Phys. Lett. **98**, 163105 (2011).

[19] I. Ramiro, E. Antolín, M.J. Steer, P.G. Linares, E. Hernández, I. Artacho, E. López, T. Ben, J.M. Ripalda, S.I.

Molina, F. Briones, C.R. Stanley, A. Martí, and A. Luque, in *Conf. Rec. IEEE Photovolt. Spec. Conf.* (2012).

[20] Í. Ramiro, J. Villa, P. Lam, S. Hatch, J. Wu, E. López, E. Antolín, H. Liu, A. Martí, and A. Luque, IEEE J. Photovoltaics **5**, (2015).

[21] C. Schneider, S. Kremling, N. V Tarakina, T. Braun, M. Adams, M. Lermer, S. Reitzenstein, L. Worschech, M. Kamp, and S. Höfling, Semicond. Sci. Technol. **27**, 32002 (2012).

[22] P. Lam, J. Wu, M. Tang, D. Kim, S. Hatch, I. Ramiro, V.G. Dorogan, M. Benamara, Y.I. Mazur, G.J. Salamo, J. Wilson, R. Allison, and H. Liu, Sol. Energy Mater. Sol. Cells **144**, (2016).

[23] S.J. Xu, X.C. Wang, S.J. Chua, C.H. Wang, W.J. Fan, J. Jiang, and X.G. Xie, Appl. Phys. Lett. **72**, 3335 (1998).

[24] Y. Shoji and Y. Okada, in *2014 IEEE 40th Photovolt. Spec. Conf.* (IEEE, 2014), pp. 1099–1102.

[25] E. Antolín, A. Martí, C.D. Farmer, P.G. Linares, E. Hernández, A.M. Sánchez, T. Ben, S.I. Molina, C.R. Stanley, and A. Luque, J. Appl. Phys. **108**, 064513 1 (2010).

[26] I. Ramiro, E. Antolín, A. Martí, C.D. Farmer, C.R. Stanley, and A. Luque, Sol. Energy Mater. Sol. Cells **140**, (2015).

[27] K. Sablon, A. Sergeev, N. Vagidov, A. Antipov, J. Little, and V. Mitin, Nanoscale Res. Lett. **6**, 584 (2011).

[28] E. Antolín, A. Martí, P.G. Linares, I. Ramiro, E. Hernández, C.D. Farmer, C.R. Stanley, and A. Luque, in *Conf. Rec. IEEE Photovolt. Spec. Conf.* (2010).

[29] A. Luque, P.G. Linares, A. Mellor, V. Andreev, and A. Martí, Appl. Phys. Lett. **103**, 123901 (2013).

[30] P.G. Linares, E. López, I. Ramiro, A. Datas, E. Antolín, Y. Shoji, T. Sogabe, Y. Okada, A. Martí, and A. Luque, Sol. Energy Mater. Sol. Cells **132**, (2015).

[31] R.B. Laghumavarapu, A. Moscho, A. Khoshakhlagh, M. El-Emawy, L.F. Lester, and D.L. Huffaker, Appl. Phys. Lett. **90**, 173123 (2007).

[32] D. Alonso-Álvarez, B. Alén, J.M. García, and J.M. Ripalda, Appl. Phys. Lett. **91**, 263103 (2007).

[33] P.J. Carrington, A.S. Mahajumi, M.C. Wagener, J.R. Botha, Q. Zhuang, and A. Krier, Phys. B Condens. Matter **407**, 1493 (2012).

[34] M.C. Wagener, P.J. Carrington, J.R. Botha, and A. Krier, J. Appl. Phys. **116**, 44304 (2014).

[35] J. Hwang, K. Lee, A. Teran, S. Forrest, J.D. Phillips, A.J. Martin, and J. Millunchick, Phys. Rev. Appl. **1**, 051003 (2014).

[36] I. Ramiro, E. Antolín, J. Hwang, A. Teran, A.J. Martin, P.G. Linares, J. Millunchick, J. Philips, A. Martí, and A. Luque, IEEE J. Photovoltaics **7**, 508 (2017).

[37] C.G. Van de Walle, Phys. Rev. B **39**, 1871 (1989).

[38] F. Hatami, N.N. Ledentsov, M. Grundmann, J. Böhrer, F. Heinrichsdorff, M. Beer, D. Bimberg, S.S. Ruvimov, P.

Werner, U. Gösele, J. Heydenreich, U. Richter, S. V Ivanov, B.Y. Meltser, P.S. Kop'ev, and Z.I. Alferov, Appl. Phys. Lett. **67**, 656 (1995).

[39] K. Suzuki, R.A. Hogg, and Y. Arakawa, J. Appl. Phys. **85**, 8349 (1999).

[40] R. Timm, H. Eisele, A. Lenz, S.K. Becker, J. Grabowski, T.-Y. Kim, L. Müller-Kirsch, K. Pötschke, U.W. Pohl, D. Bimberg, and M. Dähne, Appl. Phys. Lett. **85**, 5890 (2004).

[41] A.J. Martin, J. Hwang, E.A. Marquis, E. Smakman, T.W. Saucer, G. V Rodriguez, A.H. Hunter, V. Sih, P.M. Koenraad, and J.D. Phillips, Appl. Phys. Lett. **102**, 113103 (2013).

[42] F. Hatami, M. Grundmann, N.N. Ledentsov, F. Heinrichsdorff, R. Heitz, J. Böhrer, D. Bimberg, S.S. Ruvimov, P. Werner, V.M. Ustinov, P. S. Kop'ev, and Zh. I. Alferov, Phys. Rev. B **57**, 4635 (1998).

[43] C. Sun, G. Wang, J.E. Bowers, B. Brar, H. Blank, H. Kroemer, and M.H. Pilkuhn, Appl. Phys. Lett. **68**, 1543 (1996).

[44] T. Nowozin, A. Marent, L. Bonato, A. Schliwa, D. Bimberg, E.P. Smakman, J.K. Garleff, P.M. Koenraad, R.J. Young, and M. Hayne, Phys. Rev. B **86**, 035305 (2012).

[45] M.C. Wagener, P.J. Carrington, J.R. Botha, and A. Krier, J. Appl. Phys. **115**, 14302 (2015).

[46] M. Geller, C. Kapteyn, L. Muller-Kirsch, R. Heitz, and D. Bimberg, Appl. Phys. Lett. **82**, 2706 (2003).

[47] B.E. Sernelius, Phys. Rev. B **33**, 8582 (1986).

[48] G. Borghs, K. Bhattacharyya, K. Deneffe, P. Van Mieghem, and R. Mertens, J. Appl. Phys. **66**, 4381 (1989).

[49] Y. Toda, O. Moriwaki, M. Nishioka, and Y. Arakawa, Phys. Rev. Lett. **82**, 4114 (1999).

[50] P.G. Linares, A. Martí, E. Antolín, C.D. Farmer, I. Ramiro, C.R. Stanley, and A. Luque, Sol. Energy Mater. Sol. Cells **98**, (2012).

[51] G. Jolley, L. Fu, H.F. Lu, H.H. Tan, and C. Jagadish, Prog. Photovoltaics Res. Appl. **21**, 736 (2013).

[52] A. Luque, A. Mellor, I. Tobías, E. Antolín, P.G. Linares, I. Ramiro, and A. Martí, Phys. B Condens. Matter **413**, (2013).

[53] S. Sanguinetti, M. Henini, M. Grassi Alessi, M. Capizzi, P. Frigeri, and S. Franchi, Phys. Rev. B **60**, 8276 (1999).

[54] T. Kita, T. Maeda, and Y. Harada, Phys. Rev. B **86**, 035301 (2012).

[55] D.A.B. Miller, D.S. Chemla, T.C. Damen, A.C. Gossard, W. Wiegmann, T.H. Wood, and C.A. Burrus, Phys. Rev. Lett. **53**, 2173 (1984).

[56] D.A.B. Miller, D.S. Chemla, T.C. Damen, A.C. Gossard, W. Wiegmann, T.H. Wood, and C.A. Burrus, Phys. Rev. B **32**, 1043 (1985).

[57] C. Tablero, J. Chem. Phys. **122**, 64701 (2005).

[58] C. Tablero, J. Appl. Phys. **106**, 74306 (2009).

[59] C.E. Pryor and M.E. Pistol, Phys. Rev. B **72**, 205311 (2005).

[60] M. Grundmann, O. Stier, and D. Bimberg, Phys. Rev. B **52**, 11969 (1995).

[61] M. Califano and P. Harrison, Phys. Rev. B **61**, 10959 (2000).

[62] S.-H. Wei and A. Zunger, Appl. Phys. Lett. **72**, 2011 (1998).

[63] Y. Hinuma, A. Grüneis, G. Kresse, and F. Oba, Phys. Rev. B **90**, 155405 (2014).

[64] A. Luque and A. Martí, Prog. Photovoltaics Res. Appl. **9**, 73 (2001).

[65] A. Mellor, A. Luque, I. Tobías, and A. Martí, Sol. Energy Mater. Sol. Cells **130**, 225 (2014).

[66] M.J. Mendes, E. Hernández, E. López, P. García-Linares, I. Ramiro, I. Artacho, E. Antolín, I. Tobías, A. Martí, and A. Luque, Nanotechnology **24**, (2013).